

Analysis of long-term precipitation pattern over Antarctica derived from satellite-borne radar

L. Milani et al.

Analysis of long-term precipitation pattern over Antarctica derived from satellite-borne radar

L. Milani¹, F. Porcù², D. Casella¹, S. Dietrich¹, G. Panegrossi¹, M. Petracca^{1,2}, and P. Sanò¹

¹Institute for the Sciences of the Atmosphere and Climate, National Council of Research, Rome, Italy

²Department of Physics and Earth Sciences – University of Ferrara, Ferrara, Italy

Received: 3 December 2014 – Accepted: 8 December 2014 – Published: 8 January 2015

Correspondence to: L. Milani (lisa.milani.work@gmail.com)

Published by Copernicus Publications on behalf of the European Geosciences Union.

This discussion paper is/has been under review for the journal The Cryosphere (TC). Please refer to the corresponding final paper in TC if available.

Title Page

Abstract

Introduction

Conclusions

References

Tables

Figures

◀

▶

◀

▶

Back

Close

Full Screen / Esc

Printer-friendly Version

Interactive Discussion

Abstract

Mass accumulation is a key geophysical parameter in understanding the Antarctic climate and its role in the global system. The local mass variation is driven by a number of different mechanisms: the deposition of snow and ice crystals on the surface from the atmosphere is generally modified by strong surface winds and variations in temperature and humidity at the ground, making it difficult to measure directly the accumulation by a sparse network of ground based instruments. Moreover, the low cloud total water/ice content and the varying radiative properties of the ground pose problems in the retrieval of precipitation from passive space-borne sensors at all frequencies. Finally, numerical models, despite their high spatial and temporal resolution, show discordant results and are difficult to be validated using ground-based measurements.

A significant improvement in the knowledge of the atmospheric contribution to the mass balance over Antarctica is possible by using active space-borne instruments, such as the Cloud Profiling Radar (CPR) on board the low earth orbit CloudSat satellite, launched in 2006 and still operating. The radar measures the vertical profile of reflectivity at 94 GHz (sensitive to small ice particles) providing narrow vertical cross-sections of clouds along the satellite track.

The aim of this work is to show that, after accounting for the characteristics of precipitation and the effect of surface on reflectivity in Antarctica, the CPR can retrieve snowfall rates on a single event temporal scale. Furthermore, the CPR, despite its limited temporal and spatial sampling capabilities, also effectively observes the annual snowfall cycle in this region. Two years of CloudSat data over Antarctica are analyzed and converted in water equivalent snowfall rate. Two different approaches for precipitation estimates are considered in this work. The results are analyzed in terms of annual and monthly averages, as well as in terms of instantaneous values. The derived snowfall maps are compared with ERA-Interim reanalysis and with in situ measurements, showing overall agreement. The effects of coastlines in enhancing precipitation rates and cloud precipitation efficiency are recognized. A significant seasonal signal also

TCD

9, 141–182, 2015

Analysis of long-term precipitation pattern over Antarctica derived from satellite-borne radar

L. Milani et al.

Title Page

Abstract

Introduction

Conclusions

References

Tables

Figures

◀

▶

◀

▶

Back

Close

Full Screen / Esc

Printer-friendly Version

Interactive Discussion



frames necessary to study precipitation characteristics. Recently, an experimental site devoted to the intensive study of clouds and precipitation microphysics has been established (Gorodetskaya et al., 2014).

The use of numerical models, in general, shows discordant results, with large bias and relatively high errors if compared with ground measurements (Gentson and Krinner, 2001). Modeled precipitation fields, however, are still extremely valuable to assess annual trends for climatic studies (Bromwich et al., 2011). At finer scales, the polar version of the MM5 model (Guo et al., 2003), has been applied to infer spatial and temporal distribution of Antarctic precipitation (Bromwich et al., 2004), addressing also the role of blowing snow. Also the RACMO2 regional atmospheric climate model has recently updated its physical package giving some improvements on Surface Energy Balance, including precipitation (Van Wessem et al., 2014).

The detection from passive space-borne Low Earth Orbiting (LEO) sensors of light and solid precipitation is made difficult over Antarctica at any wavelength, due to the highly reflecting and emitting cold background and the relatively low ice content of the clouds. Several theoretical studies have been carried out to analyze the potential of passive microwave observations to detect and retrieve snowfall and to relate microphysical properties of iced hydrometeors to the observations (e.g., Skofronick-Jackson and Johnson, 2011; Munchak and Skofronick-Jackson, 2014). The use of high frequency channels (> 150 GHz) is promising, but it is complicated by their sensitivity to the highly variable microphysical characteristics of iced hydrometeors (shape, size and density) (e.g., Johnson et al., 2012). The use of passive microwave radiometry based on the use of water vapor absorption band channels (183 GHz) (e.g., Surussavadee and Staelin, 2009; Laviola and Levizzani, 2011), less sensitive to background signal, is a valuable choice at lower latitudes, but in Antarctica it is complicated by the extremely dry atmospheric conditions. Dedicated studies on the potential of these techniques for snowfall detection and/or retrieval in the polar regions are missing. Given the sensitivity of microwave radiation to the type of snow or ice at the ground, an alternative approach was attempted to evaluate the occurrence of snowfall by the changing radia-

Analysis of long-term precipitation pattern over Antarctica derived from satellite-borne radar

L. Milani et al.

Title Page

Abstract

Introduction

Conclusions

References

Tables

Figures



Back

Close

Full Screen / Esc

Printer-friendly Version

Interactive Discussion



Analysis of long-term precipitation pattern over Antarctica derived from satellite-borne radar

L. Milani et al.

Title Page

Abstract

Introduction

Conclusions

References

Tables

Figures

◀

▶

◀

▶

Back

Close

Full Screen / Esc

Printer-friendly Version

Interactive Discussion

tive properties of the ground surface (Bindschadler et al., 2005) but without providing indication of the amount of snow accumulated. Great advances in the detection and retrieval of snowfall from space are foreseen with the launch of the Global Precipitation Measurement Mission core satellite (Hou et al., 2014), but only latitudes between 65° S and 65° N will be covered.

A new tool for clouds and precipitation remote sensing at high latitudes became available with the launch of the Cloud Profiling Radar (CPR) onboard the low earth orbit CloudSat satellite in 2006. The W-band, nadir pointing radar is designed to provide vertical profiles of reflectivity of the atmosphere, allowing a physical retrieval of the vertical structure of clouds and precipitation (Stephens et al., 2002; Liu, 2008), and, under some assumptions, the quantitative estimate of the snowfall rate near the ground (Hudak et al., 2008; Liu, 2008; Kulie and Bennartz, 2009). After the first operational year of CloudSat, some studies have been done over the Antarctic region and Liu (2008) and Hiley et al. (2011) showed the first remotely sensed precipitation maps, together with extensive discussion on the Antarctic snowfall estimate using CloudSat data. Since early 2013, the CloudSat Project releases a global product (2C-SNOW-PROFILE) where the “near surface” snowfall rate is reported for each CPR profile (Wood, 2013), and these data were used by Palerme et al. (2014) to compute a multi-year precipitation map of the Antarctica ice sheet.

Along this line, we used the snowfall rate retrieval algorithm from Kulie and Bennartz (2009) from raw CPR reflectivity data, tailored to the characteristics of the Antarctic precipitation and to account for the highly reflecting background surface, obtaining a precipitation product suited for Antarctica. Furthermore, we used the 2C-SNOW-PROFILE product to extend the Palerme et al. (2014) precipitation analysis over the ocean. We analyzed two years of data (2009 and 2010) and studied the spatial distribution of annual snow amount, also as function of cloud cover. The results were compared with ERA-Interim (Dee et al., 2011) reanalysis and with the data from 6 Acoustic Depth Gauges (ADG) available at the ground. ADG data are also compared to single snowfall events, showing consistency between the CPR snowfall retrievals and the ground-

ily precipitating conditions, but attenuation effects are generally limited in drier, colder environments like Antarctica. The CPR's minimum detectable signal (around -26 dBZ) allows it to be very sensitive to light precipitation (Haynes et al., 2009), making the CPR the most reliable orbiting instrument covering all latitudes, including the polar regions, to effectively detect and retrieve snowfall distribution and intensity (Liu, 2008), with an accuracy comparable with ground based observations (Matrosov et al., 2008; Hudak et al., 2008).

Two years of CloudSat CPR data from January 2009 to December 2010, hereafter referred to as Observing Period (OP), are considered in this study. A significant gap, due to CPR battery problems, occurred from 7 December 2009 to 16 January 2010 reducing the number of satellite tracks to 9541 (about 560 tracks less than the expected number). We selected the area south of 60° S. Figure 1 shows the map of the daily frequency of CloudSat overpasses, averaged over the OP, and sampled over 1° latitude by 1.5° longitude wide grid boxes. Over continental Antarctica the daily frequency ranges between 0.3 to 1.3 overpasses per day, while there is an average of 1 overpass every 3 to 10 days over oceanic regions.

The CPR data used in this work are the radar reflectivity factor vertical profiles, hereafter referred to as reflectivity (Z), as released in the 2B-GEOPROF product (Mace, 2007), where the complete data navigation and geolocation are also present. The CPR_echo_top data (also present in the 2B-GEOPROF product), providing information on the cloud top height and on cloud type (low, middle, high or multi layer), is also used to analyze cloud cover and properties related to snowfall episodes. A data quality flag is also delivered in 2B-GEOPROF and we considered only profiles with the highest quality. Together with 2B-GEOPROF product, surface snowfall rate retrievals from the 2C-SNOW-PROFILE product (Wood, 2013) are also used. It has to be mentioned that these products are "global", i.e. no particular adaptation to the Antarctic environment is applied to the products. In addition, the CloudSat ECMWF-AUX product is used, where the two-meter temperature is provided together with other ancillary ECMWF state variable data interpolated to each CloudSat CPR footprint.

Analysis of long-term precipitation pattern over Antarctica derived from satellite-borne radar

L. Milani et al.

Title Page

Abstract

Introduction

Conclusions

References

Tables

Figures

◀

▶

◀

▶

Back

Close

Full Screen / Esc

Printer-friendly Version

Interactive Discussion



2.1.1 Kulie and Bennartz (2009) snowfall rate retrieval algorithm.

The algorithm here considered to retrieve snowfall properties over Antarctica is based on the technique developed by Kulie and Bennartz (2009) (hereafter referred as KB09) that makes use of CPR reflectivity profiles to select clouds with precipitation and then assigns a snowfall rate to the profiles. The algorithm first selects profiles with near-surface reflectivity (Z) (i.e., the reflectivity of the 6th bin from the ground, around 1200 m above the surface) above -15 dBZ, and a continuous vertical layer of reflectivity exceeding -15 dBZ in at least 5 contiguous bins. After a comparison with ECMWF-AUX temperature field, profiles with 2 m temperature higher than 0°C are screened out, in order to consider only profiles with potentially dry snow. The selected profiles are candidate snowfall profiles and the snowfall rate (S) is computed by applying a suitable Z – S relationship to the reflectivity of the near-surface bin. A more detailed description of the algorithm can be found in Kulie and Bennartz (2009).

A further study (Hiley et al., 2011) addressed the sensitivity of the algorithm to the choice of some parameters, such as the depth of the cloud vertical continuity, the reflectivity thresholds, and the parameters of the Z – S relationship, among others.

Several values of the a and b coefficients in the Z – S formula (in the form of $Z = aS^b$, where Z is in $\text{mm}^6 \text{m}^{-3}$ and S is the water equivalent snowfall rate in mm h^{-1}) are proposed in the literature and a summary can be found in Hiley et al. (2011). Some experimental studies reported on the microphysical properties of precipitating ice particles finding average effective radius (area-weighted mean radius) around $24 \mu\text{m}$ (Walden et al., 2003) and recognizing the bulk of precipitation as due to columns and bullets and aggregates of them, with sizes varying at different experimental sites (Bromwich, 1988). Given the little information available on shape and size distribution of ice cloud and precipitation particles over Antarctica, we used a and b averaged values, computed as a best fit by considering 20 different Z – S relationships found in the literature, following Hiley et al. (2011). Two other pairs of coefficients are introduced in order to

Analysis of long-term precipitation pattern over Antarctica derived from satellite-borne radar

L. Milani et al.

Title Page

Abstract

Introduction

Conclusions

References

Tables

Figures

◀

▶

◀

▶

Back

Close

Full Screen / Esc

Printer-friendly Version

Interactive Discussion



Analysis of long-term precipitation pattern over Antarctica derived from satellite-borne radar

L. Milani et al.

Title Page

Abstract

Introduction

Conclusions

References

Tables

Figures

◀

▶

◀

▶

Back

Close

Full Screen / Esc

Printer-friendly Version

Interactive Discussion



uct does not consider the bins below the 3rd bin from the surface if the profile is over ocean without sea ice, or over inland water, and below the 5th bin if the profile is over land, sea ice, or unknown surface. Also in this case a reflectivity threshold of -15 dBZ is applied to the near surface bin to separate snowing from not snowing profiles. Together with geolocation and snowfall rate variables, the product provides a retrieval status flag (snow_retrieval_status, SRS flag). This flag needs to be taken into account when using the snowfall rate data. The bit 3 of the SRS binary value is active when the snowfall rate at the base of the snow layer is substantially larger than that in the profile bin immediately above and this could be an indication of the effects of surface clutter, shallow precipitation, or partial melting of the snow. The developers suggest to use this profiles with caution and in cases where users conclude that the profile may be affected by ground clutter, the retrieval results for the bin above the near-surface bin may be used instead.

After a deeper investigation of the SRS flag behavior over Antarctica, we found that profiles with SRS bit 3 active are affected by ground clutter and are then corrected using the snowrate value of the bin immediately above the near surface bin. In Fig. 3 the PDF of the reflectivity used in the 2C-SNOW product retrieval is shown (black line), together with the PDF of profiles marked as affected by ground clutter (red line) from the 2C-SNOW product. As for the KB09 algorithm, the number of bins affected by ground clutter is not very high (also in this case only 10^{-5} of total profiles within the OP), but enough to affect mean snowfall rate values (the annual mean snowfall rate decreases 1.3% over the total Antarctic region, but more than 9.6% if we consider only the grounded ice sheet below 2000 m where the ground clutter contamination is expected to be higher).

The optimal $Z-S$ relationship is in this case dynamic and is calculated by minimizing a cost function which represents differences between simulated and observed reflectivities and also between estimated and a priori values for the snow microphysical properties (further details can be found in Wood, 2013).

2.2 Ground data: the Acoustic Depth Gauges

Long term ground based precipitation measurements over Antarctica rely on a sparse number of stations equipped with heated raingauges and/or Acoustic Depth Gauges (ADG), the latter measuring the distance from the snow covered surface to the instrument. Both instruments have strong limitations when a reliable measure of snowfall rate is needed (Eisen et al., 2008). For raingauge measurements in polar regions most of the uncertainties are related to wetting, evaporation losses, and strong winds (Sugiura et al., 2003): in particular winds induce undercatch, but also an overestimation bias due to blowing snow. The relative impact of these two effects depends on the type of wind-shield used. The measure of accumulated snow by ADG is influenced by many other factors than precipitation itself, since other different processes can change the height of the snow at the ground: blowing snow, deposition of hoar frost, surface sublimation, snowdrift sublimation, snow settling and compaction over time, meltwater (Knuth et al., 2010; Li and Pomeroy, 1997).

In this work we make use of the data from 6 ADG stations, whose location is shown in Fig. 4, managed by the University of Wisconsin-Madison Automatic Weather Station Program during the OP (Knuth et al., 2010). We processed the ADG 10 min data in order to evaluate the snow amount accumulated at the ground at two different time scales, monthly and at the single snowfall event time scale. The monthly distance variation between instrument and snow covered ground is computed by subtracting the ADG distance measurement at the end of the month by the one at the beginning of the month. The distance at the beginning (and at the end) of each month is computed as the mean distance over the first (last) five days of the month and the last (first) five days of the previous (following) month. After the screening of the outliers (i.e. very large distance variations over 10 min) we obtained the monthly distance variation which corresponds to a variation of the snow accumulation between the end and the beginning of each month of the OP: a positive ADG distance variation for one month indicates that a decrease of the accumulated snow occurred (negative snow accumulation variation,

TCD

9, 141–182, 2015

Analysis of long-term precipitation pattern over Antarctica derived from satellite-borne radar

L. Milani et al.

Title Page

Abstract

Introduction

Conclusions

References

Tables

Figures

◀

▶

◀

▶

Back

Close

Full Screen / Esc

Printer-friendly Version

Interactive Discussion



Analysis of long-term precipitation pattern over Antarctica derived from satellite-borne radar

L. Milani et al.

Title Page

Abstract

Introduction

Conclusions

References

Tables

Figures

◀

▶

◀

▶

Back

Close

Full Screen / Esc

Printer-friendly Version

Interactive Discussion

i.e., average snow accumulation at the end of the month less than average accumulation at the beginning of the month), while a negative ADG distance value is related to an increase of the accumulation (positive snow accumulation variation, i.e., average snow accumulation at the end of the month more than average accumulation at the beginning of the month).

CloudSat has overpasses within a 10 km radius of 5 of the 6 ADG stations, for which a comparison at the single snowfall event scale is possible. The distance variation at the time of a CPR overpass for a given station (hereafter, instantaneous distance variation) is computed as the difference between the average distance computed over the 5 h following the time of the overpass, and the average distance over the 5 h preceding the overpass. This relatively long time slot was necessary in order to have a minimum number of observations to compute the average, considering the high number of missing data and outliers.

3 Results

The analysis of solid precipitation over Antarctica and surrounding ocean is carried out at two different spatial and temporal resolutions. The CPR retrievals (both KB09 and 2C-SNOW) are analyzed at the CPR footprint scale, discussing statistical properties of snowrate at the highest resolution available. A parallel analysis is performed, sampling the CPR data on 1° (in latitude) by 1.5° (in longitude) wide grid boxes, where monthly and annual cumulated snow amounts are computed.

3.1 Analysis of annual gridded snowfall pattern

As first result, we computed the mean snowfall rate over the OP, expressed in mm of water equivalent per year, estimated in each $1^\circ \times 1.5^\circ$ grid box: the sum of all instantaneous snowfall rate estimates (in mm h^{-1}) divided by the total number of observations (i.e. number of CPR profiles) over the whole OP within each grid box. The mean snow-

fall rate in mmh^{-1} is then reported in mmyr^{-1} . Figure 5a shows the result obtained using the AVE values for the coefficients a and b in the $Z-S$ relationship for KB09 (see Table 1). The same map is shown for 2C-SNOW in Fig. 5b. In Fig. 5c the correspondent quantity as computed by the ECMWF ERA-Interim (ERA-I) reanalysis is shown, considering the original 12 hourly snowfall field data (provided in m of equivalent water), at $0.25^\circ \times 0.25^\circ$ spatial resolution (Dee et al., 2011), interpolated onto the $1^\circ \times 1.5^\circ$ grid, and summed over the entire OP. The total cumulated snowfall for the entire OP has been divided by 2 (years) to obtain the mean snowfall per year to be compared to the mean snowfall rate derived from CPR (all the three expressed in mmyr^{-1}). We considered here ERA-I as a reference to assess the order of magnitude of our estimates as the only available spatially distributed snowfall fields over Antarctica. As for KB09 retrievals, the comparison indicates that the choice of the AVE values for the a and b coefficients is appropriate, while the comparison with estimated maps obtained by using $\text{AVE} + \sigma$ and $\text{AVE} - \sigma$ (not shown here) presents marked under- and over-estimation, respectively, with respect to the ERA-I map.

Comparing the estimate maps with the forecast reanalysis map, the first distinguishing feature is that the order of magnitude of the mean annual snowfall rate is very similar over the grounded ice sheet for both CloudSat-based methodologies. The KB09 estimates, however, exhibit a larger extension of the very dry area (snowfall rate below 50mmyr^{-1}) that approaches the coastlines. The 2C-SNOW estimates better describe the precipitation pattern showing, similarly to the ERA-I reanalysis, more precipitation along the coasts, especially along the western side of the Antarctic Peninsula. However, it is worth noting that both the satellite estimates locate a clear maximum over the western tip of the Peninsula (yellow areas), also shown in the reanalysis. Over the ocean the KB09 shows a precipitation pattern very similar to the ERA-I one, with some discrepancies in the spatial distribution and extension of local minima and maxima. A relative maxima is found in both maps over the eastern ocean, around 60°E and between 110 and 150°E . On the other hand, 2C-SNOW, over the ocean, shows a very high precipitation amount if compared to ERA-I values. This behavior could be

Analysis of long-term precipitation pattern over Antarctica derived from satellite-borne radar

L. Milani et al.

Title Page

Abstract

Introduction

Conclusions

References

Tables

Figures

◀

▶

◀

▶

Back

Close

Full Screen / Esc

Printer-friendly Version

Interactive Discussion

Analysis of long-term precipitation pattern over Antarctica derived from satellite-borne radar

L. Milani et al.

Title Page

Abstract

Introduction

Conclusions

References

Tables

Figures

◀

▶

◀

▶

Back

Close

Full Screen / Esc

Printer-friendly Version

Interactive Discussion



primarily due to the different approach used to determine mixed precipitation in ERA-I and in 2C-SNOW. As a matter of fact, if we compare the 2C-SNOW map and the “Total Precipitation” field of ERA-I the two become very similar (see Fig. 5d). On the other hand, it is worth noting that only the contribution of dry snow is considered in the KB09 product. Further investigation is necessary to assess the effective contribution of wet snowfall or mixed phase to the precipitation in the 2C-SNOW product and this will be the focus of future work.

These results indicate that the CPR observation, even subject to low spatial and temporal sampling, are able to reconstruct the main features of the mean annual snowfall patterns, due also to the expected low variability of snowfall fields. The patchy snowfall pattern over the oceans, where more homogeneous fields are expected given the lack of surface forcing, could be due to the poor sampling of the CPR (see Fig. 1).

The scatterplot between ERA-I and CPR retrieved mean annual snowfall, all remapped on the $1^\circ \times 1.5^\circ$ grid are shown in Fig. 6. The KB09 estimate displays a fairly good correlation (0.89) for snowfall rate values below 400 mm yr^{-1} , with an underestimation of the CPR retrieved snowfall amount with respect to the ERA-I values. The correlation decreases for larger snowfall amounts, with a significant overestimation of the satellite values with respect to the ERA-I. The maximum value (around 1240 mm yr^{-1}) is found by the satellite technique on the Antarctic Peninsula. Small areas with a marked overestimation are mainly over the ocean at lower latitudes (especially on the west side), where the CPR sampling is particularly poor (see Fig. 1). 2C-SNOW estimates show a good global correlation due to a fairly good correlation for snowfall rate values below 400 mm yr^{-1} (0.88) and to an even acceptable correlation for larger snowfall values that however show a general overestimation with respect to ERA-I. Again maximum values are found over the Antarctic Peninsula.

3.2 Cloudiness influence on precipitation pattern

Cloudiness over Antarctica has been studied from both in situ and remote observations (Spinhirne et al., 2005; Lachlan-Cope, 2010; Bromwich et al., 2012), providing

information on cloud horizontal and vertical structures, and cloud microphysical characteristics. In this work, we use the cloud top height information of the CPR_echo_top product to compute a cloud cover map for the OP. Figure 7a shows the percentage of profiles classified as cloudy by the CPR_echo_top product (hereafter “cloud” profiles) with respect to the total number of profiles in each grid box. The cloud cover is highly correlated with topography: it is higher over the ocean and low elevation land, while is low over the Plateau. Over the ocean cloud cover patterns are more related to atmospheric circulation with a significant dependence on longitude, with wide areas, such as the Weddell Sea (around 30–50° W) and Ross Sea (around 170° W), showing lower cloud cover. Figure 7b and c show the precipitating cloud fraction, i.e., the fraction of cloudy profiles with snowfall rate larger than a minimum threshold of 0.1 mm h⁻¹ (hereafter “snow” profiles), as retrieved from KB09 and from 2C-SNOW respectively. For each grid box the number of “snow” profiles is divided by the number of “cloud” profiles. Even with different percentage of “snow” profiles (due to the different constraints applied for the retrieval) the effect of topography on the cloud efficiency in producing snowfall is evident: the Plateau inhibits cloud formation and the production of significant snowfall, while the red spot on the Peninsula coastline is consistent with the maximum in the mean annual snowfall shown in Fig. 5a and b, and shows a higher potential of having precipitation in that region. The lack of precipitating clouds over the peripheral ocean area for the KB09 algorithm estimate is mainly due to the temperature restrictions applied to the algorithm and the exclusion of wet snow or mixed precipitation from the dataset.

3.3 Qualitative comparison of monthly ground based and CPR snowfall values

A comparison between satellite estimated monthly mean snowfall rate (computed in the same way as the annual mean snowfall rate, but on a monthly basis) and the measurements from the 6 ADG is performed in order to provide a qualitative measure of the accuracy of the CPR ability to detect snowfall.

Analysis of long-term precipitation pattern over Antarctica derived from satellite-borne radar

L. Milani et al.

Title Page

Abstract

Introduction

Conclusions

References

Tables

Figures

◀

▶

◀

▶

Back

Close

Full Screen / Esc

Printer-friendly Version

Interactive Discussion



The monthly distance variation from ADG, computed as described in Sect. 2.2, is compared to the mean snowfall rate (mm month^{-1}) in each grid box containing the ADG stations, and results are reported in Fig. 8 for each month of the OP.

Results from KB09 and from 2C-SNOW estimates present high qualitative similarities. The large majority of the months with snowfall (as derived from CPR) have a negative monthly distance variation measured by the ADG (positive snow accumulation variation, i.e., average accumulation at the end of the month more than average accumulation at the beginning of the month), especially for snowfall rates higher than 25 mm month^{-1} . Many months present significant negative distance variation values in correspondence with moderate or low mean snowfall rates, and here it is expected a significant contribution of blowing snow episodes (Li and Pomeroy, 1997; Knuth et al., 2010). Points with positive distance variation (i.e., negative snow accumulation variation, i.e., average accumulation at the end of the month less than average accumulation at the beginning of the month) are mainly related to low or negligible estimated mean snowfall rates. A significant exception is found for the maximum snowfall rate (around $180 \text{ mm month}^{-1}$ as estimated by KB09 and around $320 \text{ mm month}^{-1}$ as estimated by 2C-SNOW), corresponding to a positive distance variation. These values are registered for November 2010, a warm month, when ablation and snow compaction are likely to occur (Radok and Lilie, 1977; Knuth et al., 2010).

In the validation of satellite precipitation retrievals (i.e., Puca et al., 2014), often a contingency table is constructed by matching estimates with ground reference measurements, where the number of hits (when estimates and observation both detect precipitation), misses (when only observations measure precipitation), false alarms (when only the estimate detects precipitation), and correct negatives (when both do not detect precipitation) are reported. In this case, for the reasons explained in Sect. 2.2, we can not assume the distance variation as “true” representation of the precipitated snow amount. However, an inspection of the resulting contingency tables (reported in Tables 2 and 3) could help in evaluating the overall matching between the two compared fields.

Analysis of long-term precipitation pattern over Antarctica derived from satellite-borne radar

L. Milani et al.

Title Page

Abstract

Introduction

Conclusions

References

Tables

Figures

◀

▶

◀

▶

Back

Close

Full Screen / Esc

Printer-friendly Version

Interactive Discussion



Analysis of long-term precipitation pattern over Antarctica derived from satellite-borne radar

L. Milani et al.

Title Page

Abstract

Introduction

Conclusions

References

Tables

Figures

◀

▶

◀

▶

Back

Close

Full Screen / Esc

Printer-friendly Version

Interactive Discussion

We define a hit when a month with a negative distance variation (increase of the snow accumulation) corresponds to a monthly mean snowfall rate above zero, a miss when it corresponds to estimated snowfall equal to zero, a false alarm when an estimated snowfall above zero corresponds to a distance variation below or equal to zero (decrease or no variation of the snow accumulation), and the correct negatives accordingly.

From the total number of 140 couples of monthly estimates and observations (computed in the 6 grid boxes containing ADG stations for each month, with the exception of four months during the OP when ground based data are missing), few indicators can be computed to summarize the results. For both estimate algorithms, most of the grid boxes where the CPR estimate detects precipitation corresponds to an increase of the snow accumulation (78 out of 114, i.e., 68 % as estimated by KB09 and 89 out of 132, i.e. 67 % as estimated by 2C-SNOW), while 86 % (78 out of 91) of grid boxes with an increase in the snow accumulation have an estimated snowfall amount above zero as estimated by KB09 and 98 % (89 out of 91) as estimated by 2C-SNOW. The 13 KB09 and the 2 2C-SNOW cases where the increase of snow accumulation does not correspond to estimated snowfall amount above zero could be due to blowing snow episodes, carrying snow from other sites. The main error is associated to the 36 (KB09) and to the 43 cases (2C-SNOW) where snowfall amount above zero is estimated, but no increase of the snow accumulation is measured at the ground: again blowing snow (in this case removing the snow) could be an important factor, but as mentioned, many other factors contribute to the decrease (or no variation) of the snow accumulation between the end and the beginning of the month, and these mechanisms may be active in the same months where snowfall occurs. The larger occurrence of this cases for the 2C-SNOW (43) with respect to KB09 (36) could be due to the absence of a well defined temperature threshold for the 2C-SNOW snowfall estimates, including cases of mixed precipitation that are not well or not at all measured by ADG instruments.

To study the relationship between the snow accumulation as measured by the ADG instruments and the estimated snowfall rate from CPR, we performed the compari-

son also at the single event temporal scale, and the results are presented in the next Section.

3.4 Analysis of instantaneous snowfall rates at CPR profile spatial scale

A comparison between instantaneous snowfall rate estimated from CPR and snow accumulation variation at the time of the CPR overpass as measured by the 5 ADG close to the CloudSat overpasses (station n. 08915 is out of the CPR coverage) has been carried out. A total of 195 CloudSat overpasses occurred at a distance lower than 10 km from the considered stations, and 19 events with snowfall retrieved from CPR data were collected. The distance variation measured by the ADG stations around the CPR overpass is estimated as described in Sect. 2.2 and the results are summarized in Fig. 9.

As found for the monthly values, instantaneous snowfall detected by the CPR (for both algorithms) corresponds to negative variations of the distance difference for most of the cases (increase of the snow accumulation). The relatively small number of misses, i.e. cases when the satellite does not detect snowfall but the snow accumulation increases, can be attributed to blowing snow episodes. Most of the significant snowfall episodes are related to negative distance differences, with one exception (station n. 30374) when relatively high snowfall rate corresponds to slightly positive distance variation. A closer inspection of the corresponding CPR profiles (not shown) shows a marked tilting of the snow column just above the ADG, indicating a likely occurrence of strong low level winds, able to weaken the local relationship between measurements at the ground from the ADG and the retrieval from CPR from the atmospheric layers aloft.

From the analysis of annual snowfall maps it is evident a clear signal of the influence of the topography on the precipitation patterns (see Fig. 5a and b and Bromwich, 1988). For a deeper discussion of the impact of topography on snow spatial and temporal distribution we divided the domain in three different background surface classes: (1) ocean and sea ice, (2) coastal areas and lowlands and (3) plateau (hereafter ocean, land, and

Analysis of long-term precipitation pattern over Antarctica derived from satellite-borne radar

L. Milani et al.

Title Page

Abstract

Introduction

Conclusions

References

Tables

Figures

◀

▶

◀

▶

Back

Close

Full Screen / Esc

Printer-friendly Version

Interactive Discussion



plateau, respectively), according to the height above the sea level. The separation is based on the CPR elevation flag, choosing 2000 ma.s.l. as threshold to separate between land and plateau classes. The normalized PDF of instantaneous snowfall rate, as estimated by KB09 and by 2C-SNOW, is shown in Fig. 10 for the three classes, with steps of 0.1 mm h^{-1} . The normalization is made with respect to the total number of “snow” profiles, i.e., profiles with snowfall rate larger than 0.1 mm h^{-1} . The snowfall rate over the plateau is very low (more than 99% of the “snow” profiles has values below 1 mm h^{-1}), but it has to be remarked that in this area snow accumulation is mainly due to the precipitation of small crystals in clear sky conditions (Bromwich, 1988; Knuth et al., 2010), likely associated to very low rates, not detected by CPR. Ocean and land profiles have similar behavior, with maximum snowfall rate reaching the same value of 3.5 mm h^{-1} as estimated by KB09, but with a relative abundance of higher snowrates over land (above 1.4 mm h^{-1}) with respect to ocean profiles, indicating the effect of the coastline and low elevation land on the enhancement of precipitation intensity. The 2C-SNOW PDFs show a behavior similar to the KB09 PDFs but with higher snowfall rate values exceeding 5 mm h^{-1} and with the abundance of land profiles with respect to ocean profiles starting around 2 mm h^{-1} . As estimated by KB09, the mean snowrates are $3.6 \times 10^{-2} \text{ mm h}^{-1}$ for ocean, $1.7 \times 10^{-2} \text{ mm h}^{-1}$ for land, and $2.0 \times 10^{-3} \text{ mm h}^{-1}$ for the plateau, while the values become $6.2 \times 10^{-2} \text{ mm h}^{-1}$ for ocean, $3.3 \times 10^{-2} \text{ mm h}^{-1}$ for land, and $4.6 \times 10^{-3} \text{ mm h}^{-1}$ for the plateau as estimated by 2C-SNOW product.

A further analysis on CPR snowrate at single profile scale was attempted to highlight seasonal signals in the snowfall rate distribution: we computed, for each of the three surface type classes (land, ocean, and plateau) the average snowfall rate for three-month periods (MAM, JJA, SON and DJF) of the OP and the results are reported in Fig. 11. We used here the common months grouping used to define seasons (as in Bromwich, 1988), considering though that the number of daylight hours vary substantially across the months, and thus the signal due to the change of daily insolation is embedded in the seasonal cycle. Over ocean and land both snowfall products have the highest average snowfall rate in the austral autumn (MAM), in agreement with

Analysis of long-term precipitation pattern over Antarctica derived from satellite-borne radar

L. Milani et al.

Title Page

Abstract

Introduction

Conclusions

References

Tables

Figures

◀

▶

◀

▶

Back

Close

Full Screen / Esc

Printer-friendly Version

Interactive Discussion



Bromwich (1988), while the driest season is the summer (DJF). For the plateau region, the behavior is different: higher averaged snowfall rate is estimated during DJF and lower in SON.

A further investigation was focused on the estimation of the spatial extension of precipitation pattern over Antarctica. The use of point-like ground measurements allows the estimation of the duration of snowfall events (Knuth et al., 2010), but no information can be derived on the spatial extension of snowfall patterns, given the sparse distribution of ground instruments. On the other side, the CPR does not provide information about temporal features, but, from the analysis of the lengths of the track segments with snowfall, it is possible to infer the 1-D horizontal extension of the snowfall events.

Within the dataset of CloudSat orbits with detected snowfall the 1-D horizontal extension (hereafter “length”) of the event was defined as the number of contiguous CPR footprints with snowfall rate above 0.1 mm h^{-1} . Only precipitation patterns that started and ended within the same orbit are considered. The lengths are grouped into three classes: class 1 (below 10 km), class 2 (between 10 and 100 km), and class 3 (beyond 100 km) and the number of lengths in each class are normalized with respect to the total number of lengths for each of the four seasons previously defined. The resulting histograms are reported in Fig. 12. Of course, the different algorithm used to estimate the precipitation influences the length of snowfall patterns, but the overall behavior shows common results. The austral winter (JJA) reports the highest percentage of the longest snowfall patterns (average length around 53 km for KB09 and around 46 km for 2C-SNOW). This results can be associated to the findings of Knuth et al. (2010) who found in JJA the highest percentage of long lasting events (duration longer than 1 day), to establish that JJA is the season when snowfall events with longer duration and larger spatial extension are more likely to occur. Shorter lengths ($< 10 \text{ km}$) show a slightly different behavior between the two algorithms: higher percentages are found in DJF for KB09 (average length around 36 km) and in MAM for 2C-SNOW (average length around 39 km, but very close to the value for DJF). Finally, the overall higher percentage of longer snowfall patterns (10–100 km) relative to shorter patterns ($< 10 \text{ km}$)

Analysis of long-term precipitation pattern over Antarctica derived from satellite-borne radar

L. Milani et al.

Title Page

Abstract

Introduction

Conclusions

References

Tables

Figures

◀

▶

◀

▶

Back

Close

Full Screen / Esc

Printer-friendly Version

Interactive Discussion



for KB09 with respect to 2C-SNOW can be explained by the different methodology used to define the near surface bin reflectivity in the two algorithms: the higher near surface bins used in KB09 may cause missed shallow precipitation events, mainly over the ocean, leading to a loss of shorter precipitation pattern in favour of longer patterns (10–100 km).

4 Summary and conclusions

Two different approaches for snowfall rate estimate from the CloudSat W-band spaceborne Cloud Profiling Radar reflectivity profiles were applied to the Antarctic region to study solid precipitation characteristics at different spatial and temporal scales. The algorithm of Kulie and Bennartz (2009) has been used to convert CPR reflectivity profiles for the years 2009 and 2010 to instantaneous water equivalent snowfall rates. The algorithm has been tailored to the characteristics of precipitation in Antarctica. In addition, the official CloudSat 2C-SNOW-PROFILE product with different characteristics and based on different assumptions has also been considered. For both products the significant impact of ground clutter contamination in this region has been taken into account.

The instantaneous, footprint scale, retrieved snowfall rates are first up-scaled and integrated in time to obtain spatially continuous mean annual snowfall rate maps, to be compared with ERA-I reanalysis of snowfall. The KB09 map shows general agreement with the ERA-I mean annual snowfall rate map, both in terms of numerical values and spatial distribution, while the 2C-SNOW shows good agreement with the ERA-I mean annual rate map of the total precipitation. Because of the similar behavior of 2C-SNOW and ERA-I over the grounded continent (where the surface temperature is always below 0°C), we can assert that the different amount of precipitation over the ocean is mainly due to the different approach used to determine mixed precipitation in ERA-I and in 2C-SNOW. The relation between cloud cover and snowfall frequency highlights the impact of coastal orography in enhancing the snowfall occurrence. A comparison

Analysis of long-term precipitation pattern over Antarctica derived from satellite-borne radar

L. Milani et al.

Title Page

Abstract

Introduction

Conclusions

References

Tables

Figures

◀

▶

◀

▶

Back

Close

Full Screen / Esc

Printer-friendly Version

Interactive Discussion



the results to the different assumptions and methodologies (i.e., temperature threshold used, height of near surface bin, and to the $Z-S$ relationship).

This work shows that, in spite of its limited temporal and spatial sampling capabilities, CPR can be used as a valuable source of snowfall rate data in Antarctica that can be analyzed at different temporal scales, providing support to the sparse network of ground-based instruments in this region, as well as to numerical models used to simulate single snowfall events (at high temporal and spatial resolution), or used for climatological studies. CPR snowfall products tailored to the characteristic of the Antarctic region could then be used in the analysis and interpretation of passive measurements from the large number of radiometers on board polar satellites orbiting around the globe providing full spatial coverage of the whole region.

Acknowledgements. This work has been funded by the Italian Ministry of University, Research and Education under the National Plan for Antarctic Research PNRA (PEA 2009) “Bilancio della sostanza ghiaccio e caratterizzazione delle precipitazioni solide in Antartide”.

We would like to acknowledge for the use of ERA-Interim dataset produced by ECMWF and freely available at: <http://apps.ecmwf.int>

The authors appreciate the support of the University of Wisconsin-Madison Automatic Weather Station Program for the data set, data display, and information, NSF grant numbers ANT-0944018 and ANT-1245663.

Finally, we also appreciate the valuable support of Mark Kulie, Norman Wood and Tristan L’Ecuyer on the use of 2C-SNOW-PROFILE product.

References

- Arthern, R. J., Winebrenner, D. P., and Vaughan, D. G.: Antarctic snow accumulation mapped using polarization of 4.3cm wavelength microwave emission, *J. Geophys. Res.*, 111, D06107, doi:10.1029/2004JD005667, 2006.
- Bindschadler, R., Choi, H., Shuman, C., and Markus, T.: Detecting and measuring new snow accumulation on ice sheets by satellite remote sensing, *Remote Sens. Environ.*, 98, 388–402, 2005.

Analysis of long-term precipitation pattern over Antarctica derived from satellite-borne radar

L. Milani et al.

Title Page

Abstract

Introduction

Conclusions

References

Tables

Figures

◀

▶

◀

▶

Back

Close

Full Screen / Esc

Printer-friendly Version

Interactive Discussion



**Analysis of long-term
precipitation pattern
over Antarctica
derived from
satellite-borne radar**

L. Milani et al.

[Title Page](#)[Abstract](#)[Introduction](#)[Conclusions](#)[References](#)[Tables](#)[Figures](#)[◀](#)[▶](#)[◀](#)[▶](#)[Back](#)[Close](#)[Full Screen / Esc](#)[Printer-friendly Version](#)[Interactive Discussion](#)

- Bromwich, D. H.: Snowfall in high southern latitudes, *Rev. Geophys.*, 26, 149–168, 1988.
- Bromwich, D. H., Guo, Z., Bai, L., and Chen, Q.-S.: Modeled Antarctic precipitation. Part I: Spatial and temporal variability, *J. Climate*, 17, 427–447, 2004.
- Bromwich, D. H., Nicolas, J. P., and Monaghan, A. J.: An assessment of precipitation changes over Antarctica and the Southern Ocean since 1989 in contemporary global reanalysis, *J. Climate*, 24, 4189–4209, 2011.
- Bromwich, D. H., Nicolas, J. P., Hines, K. M., Kay, J. E., Key, E. L., Lazzara, M., Lubin, D., McFarquhar, G. M., Gorodetskaya, I. V., Grosvenor, D. P., Lachlan-Cope, T., and van Lipzig, N. P. M.: Tropospheric clouds in Antarctica, *Rev. Geophys.*, 50, RG1004, doi:10.1029/2011RG000363, 2012.
- Dee, D. P., Uppala, S. M., Simmons, A. J., Berrisford, P., Poli, P., Kobayashi, S., Andrae, U., Balmaseda, M. A., Balsamo, G., Bauer, P., Bechtold, P., Beljaars, A. C. M., van de Berg, L., Bidlot, J., Bormann, N., Delsol, C., Dragani, R., Fuentes, M., Geer, A. J., Haimberger, L., Healy, S. B., Hersbach, H., Hólm, E. V., Isaksen, I., Kållberg, P., Köhler, M., Matricardi, M., McNally, A. P., Monge-Sanz, B. M., Morcrette, J.-J., Park, B.-K., Peubey, C., de Rosnay, P., Tavolato, C., Thépaut J.-N., and Vitart, F.: The ERA-Interim reanalysis: configuration and performance of the data assimilation system, *Q. J. Roy. Meteor. Soc.*, 137, 553–597, doi:10.1002/qj.828, 2011.
- Eisen, O., Frezzotti, M., Genthon, C., Isaksson, E., Magand, O., Van Den Broeke, M. R., Dixon, D. A., Ekaykin, A., Holmlund, P., Kameda, T., Karlöf, L., Kaspari, S., Lipenkov, V. Y., Oerter, H., Takahashi, S., and Vaughan, D. G.: Ground-based measurements of spatial and temporal variability of snow accumulation in East Antarctica, *Rev. Geophys.*, 46, RG2001, doi:10.1029/2006RG000218, 2008.
- Genthon, C. and Krinner, G.: The Antarctic surface mass balance and systematic biases in general circulation models, *J. Geophys. Res.*, 106, 20653–20664, 2001.
- Gorodetskaya, I. V., Kneifel, S., Maahn, M., Van Tricht, K., Schween, J. H., Crewell, S., and Van Lipzig, N. P. M.: Cloud and precipitation properties from ground-based remote sensing instruments in East Antarctica, *The Cryosphere Discuss.*, 8, 4195–4241, doi:10.5194/tcd-8-4195-2014, 2014.
- Guo, Z., Bromwich, D. H., and Cassano, J. J.: Evaluation of polar MM5 simulations of Antarctic atmospheric circulation, *Mon. Weather Rev.*, 131, 384–411, doi:10.1175/1520-0493(2003)131<0384:EOPMSO>2.0.CO;2, 2003.

**Analysis of long-term
precipitation pattern
over Antarctica
derived from
satellite-borne radar**

L. Milani et al.

[Title Page](#)[Abstract](#)[Introduction](#)[Conclusions](#)[References](#)[Tables](#)[Figures](#)[◀](#)[▶](#)[◀](#)[▶](#)[Back](#)[Close](#)[Full Screen / Esc](#)[Printer-friendly Version](#)[Interactive Discussion](#)

Haynes, J., L'Ecuyer, T., Stephens, G., Miller, S., Mitrescu, C., and Tanelli, S.: Rainfall retrieval over the ocean with spaceborne W-band radar, *J. Geophys. Res.*, 114, D00A22, doi:10.1029/2008JD009973, 2009.

Hiley, M. J., Kulie, M. S., and Bennartz, R.: Uncertainty analysis for CloudSat snowfall retrievals, *J. Appl. Meteorol. Clim.*, 50, 399–418, 2011.

Hou, A. Y., Kakar, R. K., Neeck, S., Azarbarzin, A. A., Kummerow, C. D., Kojima, M., Oki, R., Nakamura, K., and Iguchi, T.: The Global Precipitation Measurement Mission, *B. Am. Meteorol. Soc.*, 95, 701–722, doi:10.1175/BAMS-D-13-00164.1, 2014.

Hudak, D., Rodriguez, P., and Donaldson, N.: Validation of the CloudSat precipitation occurrence algorithm using the Canadian C band radar network, *J. Geophys. Res.*, 113, D00A07, doi:10.1029/2008JD009992, 2008.

Johnson, B. T., Petty, G. W., and Skofronick-Jackson, G.: Microwave properties of ice-phase hydrometeors for radar and radiometers: sensitivity to model assumptions, *J. Appl. Meteorol. Clim.*, 51, 2152–2171, doi:10.1175/JAMC-D-11-0138.1, 2012.

Knuth, S. L., Tripoli, G. J., Thom, J. E., and Weidner, G.: The influence of blowing snow and precipitation on SSH change across the Ross Ice Shelf and Ross Sea Regions of Antarctica, *J. Appl. Meteorol. Clim.*, 49, 1306–1321, 2010.

Kulie, M. S. and Bennartz, R.: Utilizing spaceborne radars to retrieve dry snowfall, *J. Appl. Meteorol. Clim.*, 48, 2564–2580, 2009.

Lachlan-Cope, T.: Antarctic clouds, *Polar Res.*, 29, 150–158, 2010.

Laviola, S. and Levizzani, V.: The 183-WSL fast rainrate retrieval algorithm. Part I: Retrieval design, *Atmos. Res.*, 99, 443–461, 2011.

Li, L. and Pomeroy, J. W.: Probability of occurrence of blowing snow, *J. Geophys. Res.*, 102, 21955–21964, 1997.

Liu, G.: Deriving snow cloud characteristics from CloudSat observations, *J. Geophys. Res.*, 113, D00A09, doi:10.1029/2007JD009766, 2008.

Lubin, D. and Massom, R.: Remote sensing of Earth's polar regions – opportunities for computational science, *Comput. Sci. Eng.*, 9, 58–71, 2007.

Mace, G. G.: Level 2 GEOPROF product process description and interface control document algorithm, version 5.3., available at: <http://www.cloudsat.cira.colostate.edu/data/CDlist.php?go=list&path=/2B-GEOPROF> (last access: 6 January 2015), 2007.

Matrosov, S. Y., Shupe, M. D., and Djalalova, I. V.: Snowfall retrievals using millimeter-wavelength cloud radars, *J. Appl. Meteorol. Clim.*, 47, 769–777, 2008.

Analysis of long-term precipitation pattern over Antarctica derived from satellite-borne radar

L. Milani et al.

Title Page

Abstract

Introduction

Conclusions

References

Tables

Figures

◀

▶

◀

▶

Back

Close

Full Screen / Esc

Printer-friendly Version

Interactive Discussion



Munchak, S., and Skofronick-Jackson, G.: Evaluation of precipitation detection over various surfaces from passive microwave imagers and sounders, *Atmos. Res.*, 131, 81–94, doi:10.1016/j.atmosres.2012.10.011, 2013.

Palermé, C., Kay, J. E., Genthon, C., L'Ecuyer, T., Wood, N. B., and Claud, C.: How much snow falls on the Antarctic ice sheet?, *The Cryosphere*, 8, 1577–1587, doi:10.5194/tc-8-1577-2014, 2014.

Puca, S., Porcu, F., Rinollo, A., Vulpiani, G., Baguis, P., Balabanova, S., Campione, E., Ertürk, A., Gabellani, S., Iwanski, R., Jurašek, M., Kaňák, J., Kerényi, J., Koshinchanov, G., Kozinarova, G., Krahe, P., Lapeta, B., Lábó, E., Milani, L., Okon, L., Öztopal, A., Pagliara, P., Pignone, F., Rachimow, C., Reborá, N., Roulin, E., Sönmez, I., Toniazzo, A., Biron, D., Casella, D., Cattani, E., Dietrich, S., Di Paola, F., Laviola, S., Levizzani, V., Melfi, D., Mugnai, A., Panegrossi, G., Petracca, M., Sanò, P., Zauli, F., Rosci, P., De Leonibus, L., Agosta, E., and Gattari, F.: The validation service of the hydrological SAF geostationary and polar satellite precipitation products, *Nat. Hazards Earth Syst. Sci.*, 14, 871–889, doi:10.5194/nhess-14-871-2014, 2014.

Radok, U. and Lile, R. C.: A year of snow accumulation at Plateau Station, meteorological studies at Plateau Station, Antarctica, *Antarct. Res. Ser.*, 25, 17–26, 1977.

Skofronick-Jackson, G. and Johnson, B. T.: Thresholds of detection for falling snow from satellite-borne active and passive sensors, *Geoscience and Remote Sensing Symposium (IGARSS)*, 2011 IEEE International, Vancouver, BC, 24–29 July 2011, 2637–2640, doi:10.1109/IGARSS.2011.6049744, 2011.

Spinhirne, J. D., Palm, S. P., and Hart, W. D.: Antarctica cloud cover for October 2003 from GLAS satellite lidar profiling, *Geophys. Res. Lett.*, 32, L22S05, doi:10.1029/2005GL023782, 2005.

Stephens, G. L., Vane, D. G., Boain, R. J., Mace, G. G., Sassen, K., Wang, Z., Illingworth, A. J., O'Connor, E. J., Rossow, W. B., Durden, S. L., Miller, S. D., Austin, R. T., Benedetti, A., Mitrescu, C., and the CloudSat Science Team: The CloudSat mission and the A-Train, *B. Am. Meteorol. Soc.*, 83, 1771–1790, 2002.

Stephens, G. L., Vane, D. G., Tanelli, S., Im, E., Durden, S., Rokey, M., Reinke, D., Partain, P., Mace, G. G., Austin, R., L'Ecuyer, T., Haynes, J., Lebsock, M., Suzuki, K., Waliser, D., Wu, D., Kay, J., Gettelman, A., Wang, Z., and Marchand, R.: CloudSat mission: performance and early science after the first year of operation, *J. Geophys. Res.*, 113, D00A18, doi:10.1029/2008JD009982, 2008.

Analysis of long-term precipitation pattern over Antarctica derived from satellite-borne radar

L. Milani et al.

Title Page

Abstract

Introduction

Conclusions

References

Tables

Figures

◀

▶

◀

▶

Back

Close

Full Screen / Esc

Printer-friendly Version

Interactive Discussion



Surussavadee, C. and Staelin, D. H.: Satellite retrievals of Arctic and equatorial rain and snowfall rates using millimeter wavelengths, *IEEE T. Geosci. Remote*, 47, 3697–3707, 2009.

Sugiura, K., Yang, D., and Ohata, T.: Systematic error aspects of gauge-measured solid precipitation in the Arctic, Barrow, Alaska, *Geophys. Res. Lett.*, 30, 1–5, 2003.

5 Van Wessem, J. M., Reijmer, C. H., Morlighem, M., Mougnot, J., Rignot, E., Medley, B., Joughin, I., Wouters, B., Depoorter, M. A., Bamber, J. L., Lenaerts, J. T. M., van de Berg, W. J., van den Broeke, M. R., and van Meijgaard, E.: Improved representation of East Antarctic surface mass balance in a regional atmospheric climate model, *J. Glaciol.*, 60, 761–770, doi:10.3189/2014JoG14J051, 2014.

10 Walden, V. P., Warren, S. G., and Tuttle, E.: Atmospheric ice crystals over the Antarctic Plateau in winter, *J. Appl. Meteorol.*, 42, 1391–1405, doi:10.1175/1520-0450(2003)042<1391:AICOTA>2.0.CO;2, 2003.

15 Wood, N.: Level 2C Snow-Profile process description and interface control document, available at: <http://www.cloudsat.cira.colostate.edu/data/CDlist.php?go=list&path=/2C-SNOW-PROFILE> (last access: 6 January 2015), 2013.

Analysis of long-term precipitation pattern over Antarctica derived from satellite-borne radar

L. Milani et al.

Title Page

Abstract

Introduction

Conclusions

References

Tables

Figures

◀

▶

◀

▶

Back

Close

Full Screen / Esc

Printer-friendly Version

Interactive Discussion



Table 1. Values of the $Z = a S^b$ parameters used in this work (Z is in $\text{mm}^6 \text{m}^{-3}$ and S is the water equivalent snowfall rate in mm h^{-1}).

	AVE $- \sigma$	AVE	AVE $+ \sigma$
<i>a</i>	7.6	21.6	61.2
<i>b</i>	1.3	1.2	1.1

Analysis of long-term precipitation pattern over Antarctica derived from satellite-borne radar

L. Milani et al.

Title Page

Abstract

Introduction

Conclusions

References

Tables

Figures

◀

▶

◀

▶

Back

Close

Full Screen / Esc

Printer-friendly Version

Interactive Discussion



Table 2. Contingency table for monthly mean snowfall rate estimated by KB09 algorithm and ADG monthly distance variations (distance variation < 0 corresponds to an increase of snow accumulation, distance variation ≥ 0 corresponds to a decrease or no variation of snow accumulation).

	Monthly mean snowfall rate > 0	Monthly mean snowfall rate $= 0$
Distance variation < 0	78	13
Distance variation ≥ 0	36	13

Analysis of long-term precipitation pattern over Antarctica derived from satellite-borne radar

L. Milani et al.

Title Page

Abstract

Introduction

Conclusions

References

Tables

Figures

◀

▶

◀

▶

Back

Close

Full Screen / Esc

Printer-friendly Version

Interactive Discussion

Table 3. Contingency table for monthly mean snowfall rate estimated by 2C-SNOW product and ADG monthly distance variations (distance variation < 0 corresponds to an increase of snow accumulation, distance variation ≥ 0 corresponds to a decrease or no variation of snow accumulation).

	Monthly mean snowfall rate > 0	Monthly mean snowfall rate $= 0$
Distance variation < 0	89	2
Distance variation ≥ 0	43	6

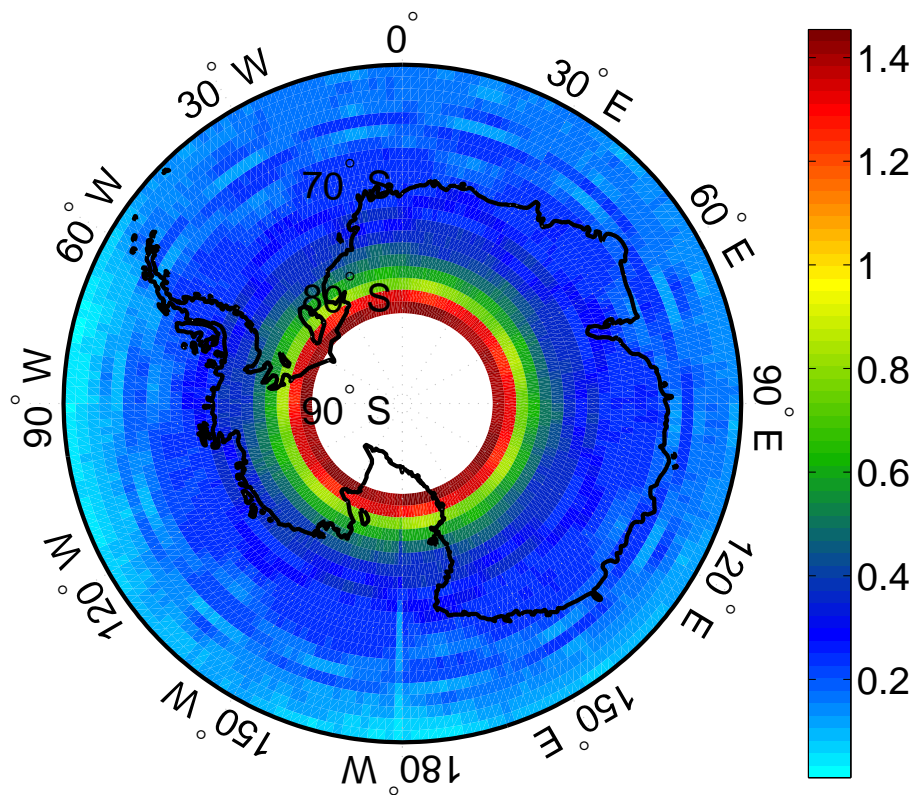


Figure 1. Averaged daily number of CloudSat CPR tracks computed over 1° latitude by 1.5° longitude wide grid boxes and averaged over the OP.

Analysis of long-term precipitation pattern over Antarctica derived from satellite-borne radar

L. Milani et al.

Title Page

Abstract Introduction

Conclusions References

Tables Figures

◀ ▶

◀ ▶

Back Close

Full Screen / Esc

Printer-friendly Version

Interactive Discussion



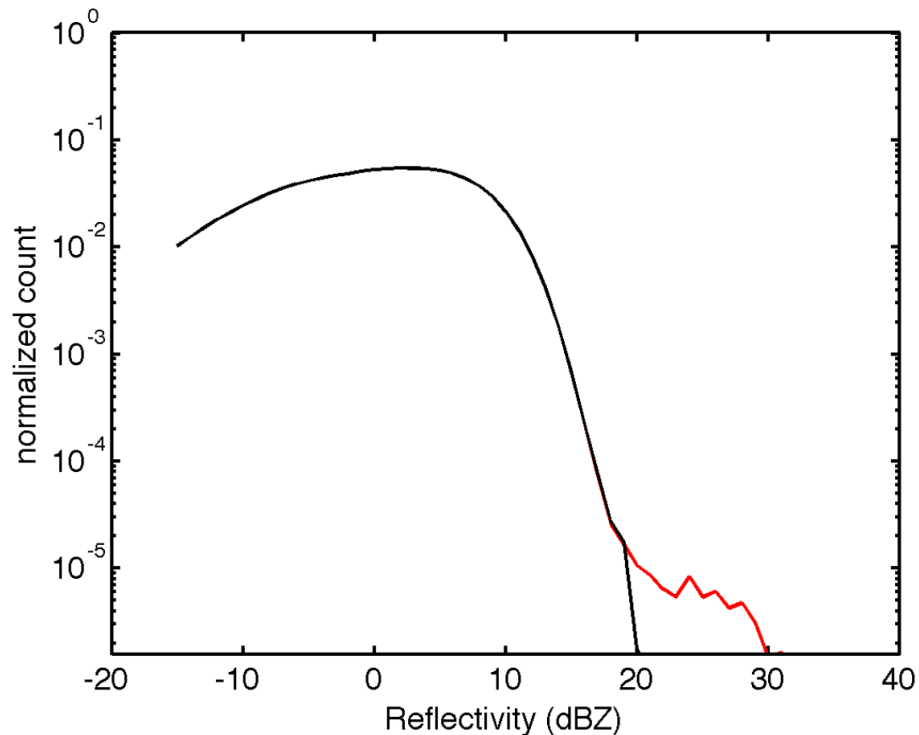


Figure 2. PDF of the reflectivity corrected for ground clutter contamination (black line). The PDF of 6th bin reflectivity for $Z > 20$ dBZ is also shown (red line). Counts are normalized to the total number of occurrences.

Analysis of long-term precipitation pattern over Antarctica derived from satellite-borne radar

L. Milani et al.

Title Page	
Abstract	Introduction
Conclusions	References
Tables	Figures
◀	▶
◀	▶
Back	Close
Full Screen / Esc	
Printer-friendly Version	
Interactive Discussion	



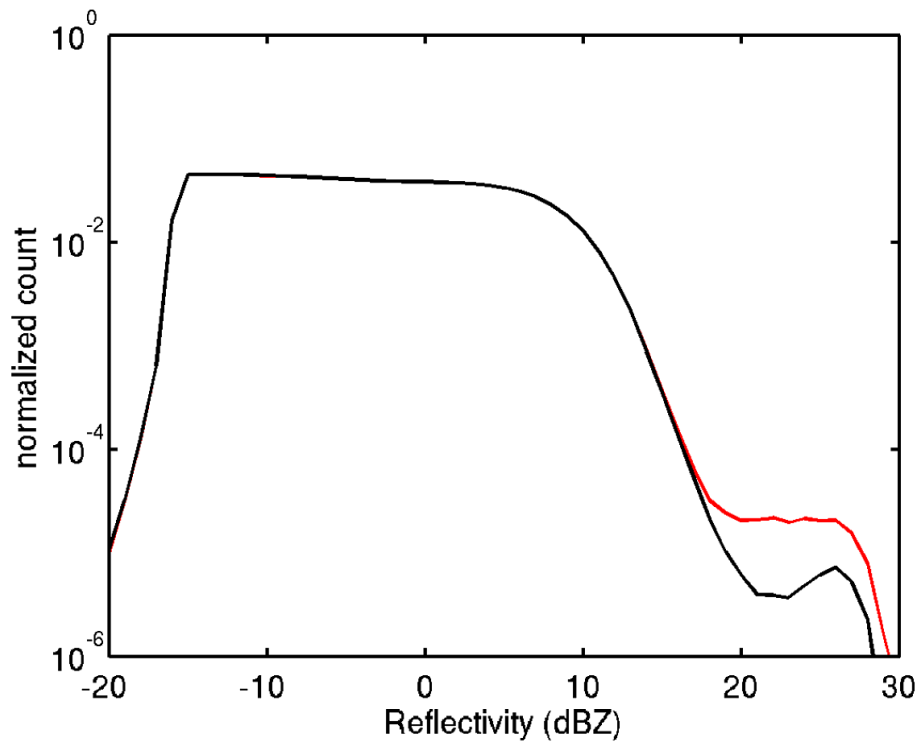


Figure 3. PDF of the near surface bin (black line) used by 2C-SNOW for the snowfall rate estimate. The PDF of the profiles with bit 3 of the SRS binary value active is also shown (red line). Counts are normalized to the total number of occurrences.

Analysis of long-term precipitation pattern over Antarctica derived from satellite-borne radar

L. Milani et al.

Title Page

Abstract Introduction

Conclusions References

Tables Figures

◀ ▶

◀ ▶

Back Close

Full Screen / Esc

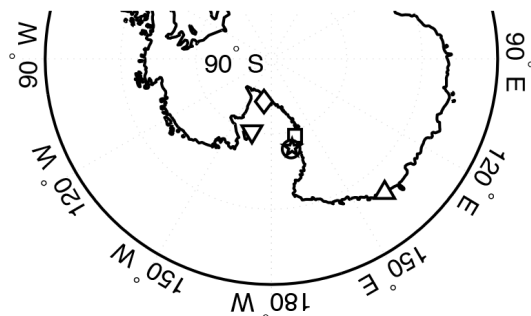
Printer-friendly Version

Interactive Discussion



Analysis of long-term precipitation pattern over Antarctica derived from satellite-borne radar

L. Milani et al.



- ▽ Margaret (08910)
- ◇ Sabrina (08915)
- Windless Bight (08982)
- * Mary (08983)
- △ Dumont D'Urville (30374)
- Willie Field (30477)

Figure 4. Location of the 6 ADG stations used in this study.

Title Page

Abstract

Introduction

Conclusions

References

Tables

Figures

◀

▶

◀

▶

Back

Close

Full Screen / Esc

Printer-friendly Version

Interactive Discussion



Analysis of long-term precipitation pattern over Antarctica derived from satellite-borne radar

L. Milani et al.

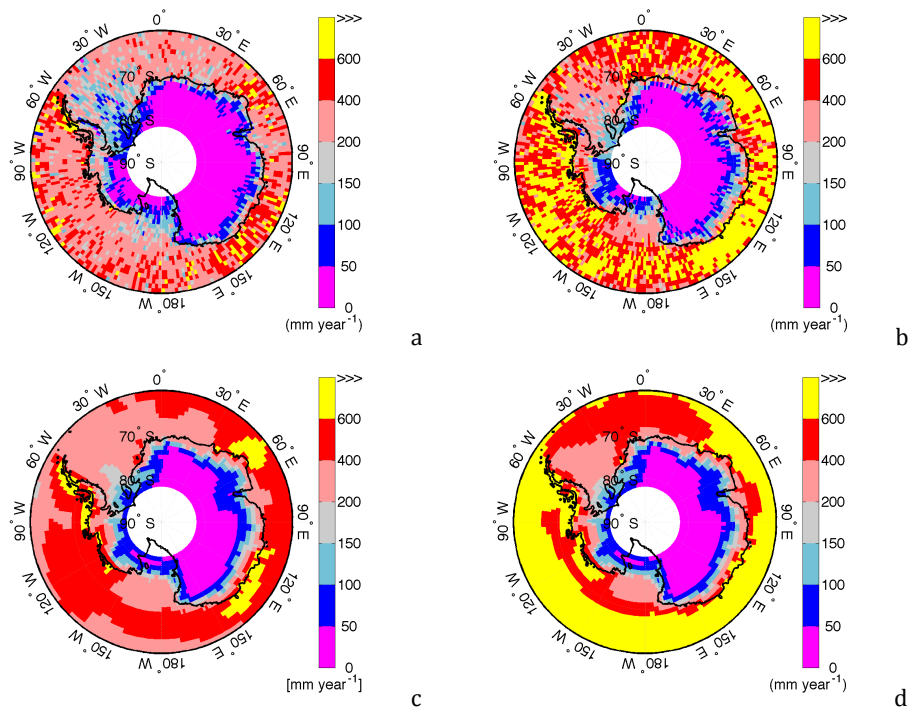


Figure 5. Mean annual snowfall rate over the Antarctica and surrounding ocean computed over the OP, as estimated by KB09 (a), as estimated by 2C-SNOW (b) and as computed by ERA-I (c) and mean annual total precipitation rate as computed by ERA-I (d).

Title Page

Abstract

Introduction

Conclusions

References

Tables

Figures

◀

▶

◀

▶

Back

Close

Full Screen / Esc

Printer-friendly Version

Interactive Discussion

Analysis of long-term precipitation pattern over Antarctica derived from satellite-borne radar

L. Milani et al.

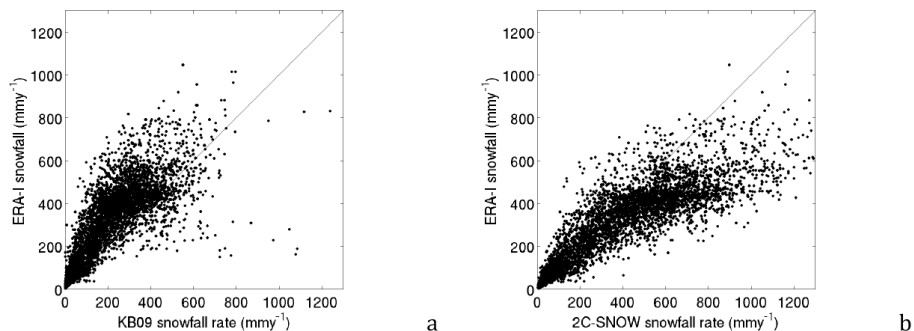


Figure 6. Scatterplot on the $1^{\circ} \times 1.5^{\circ}$ grid, between satellite retrieval as estimated by KB09 and ERA-I reanalysis **(a)**, and between 2C-SNOW product and ERA-I reanalysis **(b)**.

Title Page

Abstract

Introduction

Conclusions

References

Tables

Figures

◀

▶

◀

▶

Back

Close

Full Screen / Esc

Printer-friendly Version

Interactive Discussion

Analysis of long-term precipitation pattern over Antarctica derived from satellite-borne radar

L. Milani et al.

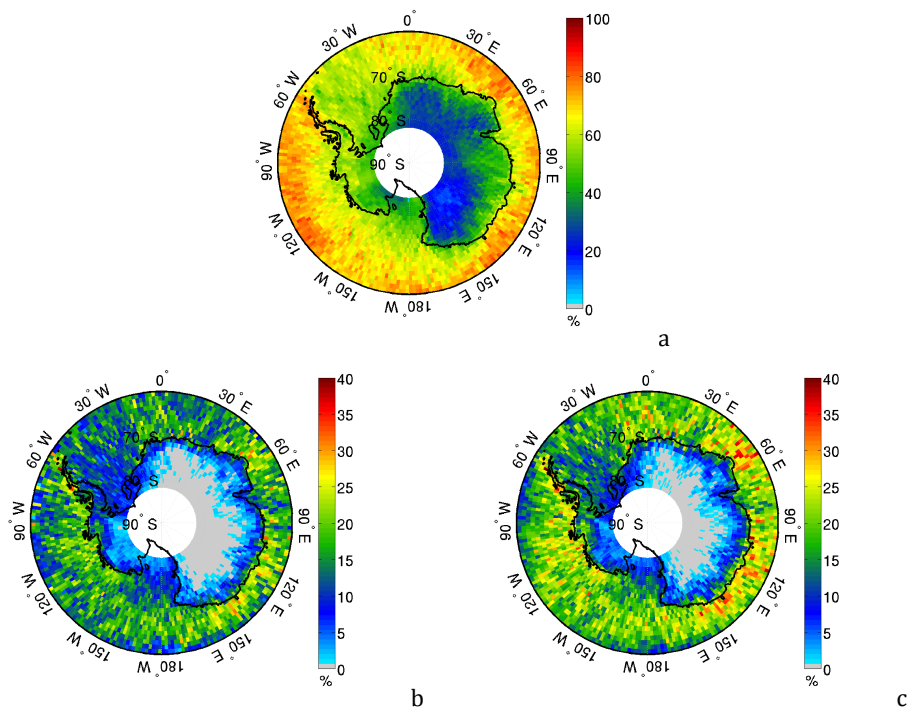


Figure 7. Maps of the cloud cover (a) and of precipitating cloud fraction calculated using KB09 (b) and 2C-SNOW (c) estimates for the OP.

[Title Page](#)[Abstract](#)[Introduction](#)[Conclusions](#)[References](#)[Tables](#)[Figures](#)[◀](#)[▶](#)[◀](#)[▶](#)[Back](#)[Close](#)[Full Screen / Esc](#)[Printer-friendly Version](#)[Interactive Discussion](#)

Analysis of long-term precipitation pattern over Antarctica derived from satellite-borne radar

L. Milani et al.

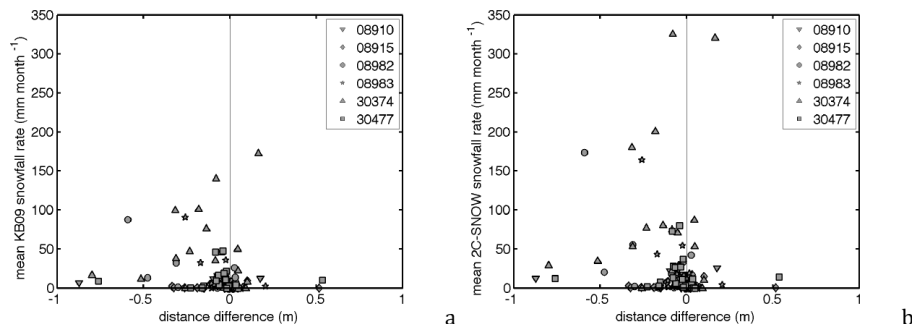


Figure 8. CPR estimated mean monthly KB09 (a) and 2C-SNOW product (b) snowfall rate as a function of the monthly distance differences for the 6 ADG stations. Symbols refer to the stations as in Fig. 4.

Title Page

Abstract

Introduction

Conclusions

References

Tables

Figures

◀

▶

◀

▶

Back

Close

Full Screen / Esc

Printer-friendly Version

Interactive Discussion

Analysis of long-term precipitation pattern over Antarctica derived from satellite-borne radar

L. Milani et al.

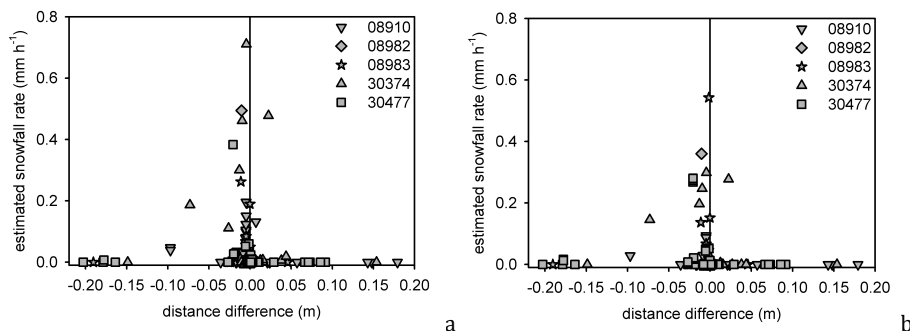


Figure 9. Estimated instantaneous KB09 (a) and 2C-SNOW (b) snowfall rate as a function of the distance variation measured by the ADG (after and before the CPR overpass, see Sect. 2.2).

Title Page

Abstract

Introduction

Conclusions

References

Tables

Figures

◀

▶

◀

▶

Back

Close

Full Screen / Esc

Printer-friendly Version

Interactive Discussion

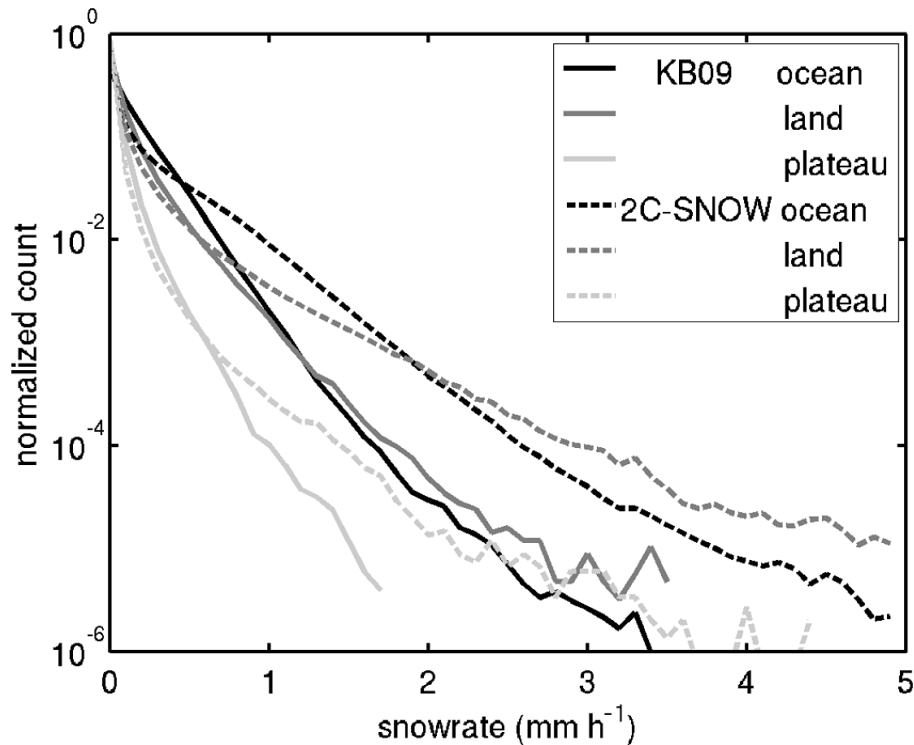


Figure 10. Normalized PDFs of the instantaneous snowfall rate as estimated by KB09 (solid lines) and by 2C-SNOW (dashed lines) for the different background surface classes.

Analysis of long-term precipitation pattern over Antarctica derived from satellite-borne radar

L. Milani et al.

Title Page

Abstract Introduction

Conclusions References

Tables Figures

◀ ▶

◀ ▶

Back Close

Full Screen / Esc

Printer-friendly Version

Interactive Discussion



Analysis of long-term precipitation pattern over Antarctica derived from satellite-borne radar

L. Milani et al.

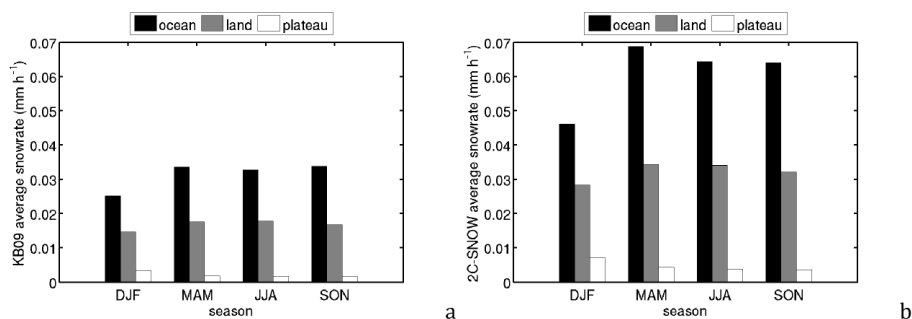


Figure 11. Average instantaneous snowfall rates as estimated by KB09 (a) and as estimated by 2C-SNOW (b) on the different surface classes for the seasons.

Title Page

Abstract

Introduction

Conclusions

References

Tables

Figures

◀

▶

◀

▶

Back

Close

Full Screen / Esc

Printer-friendly Version

Interactive Discussion

Analysis of long-term precipitation pattern over Antarctica derived from satellite-borne radar

L. Milani et al.

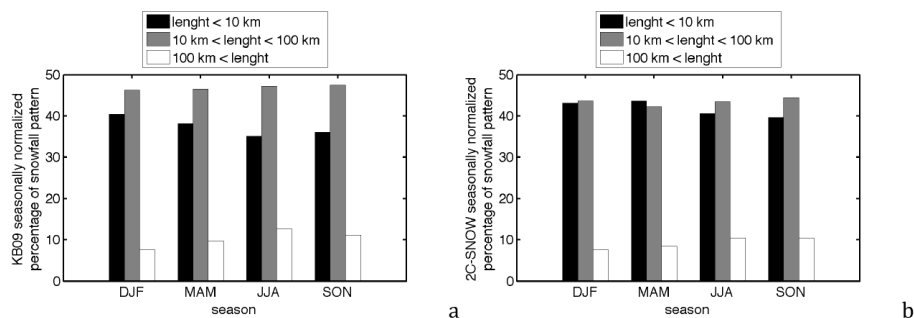


Figure 12. Distribution of continuous snowfall pattern lengths over the three length classes, normalized for the seasons, for the OP, as estimated by KB09 (a) and 2C-SNOW (b).

Title Page

Abstract

Introduction

Conclusions

References

Tables

Figures

◀

▶

◀

▶

Back

Close

Full Screen / Esc

Printer-friendly Version

Interactive Discussion